[P5]

V. Viikari, V.-M. Kolmonen, J. Salo, and A. V. Räisänen, “Antenna pattern correction technique based on an adaptive array algorithm,” accepted with minor revision for publication in *IEEE Transactions on Antennas and Propagation*, 2006.

Antenna Pattern Correction Technique Based on an Adaptive Array Algorithm

Ville Viikari, *Student Member, IEEE,* Veli-Matti Kolmonen, Jari Salo, Antti V. Räisänen, *Fellow, IEEE*

***Abstract*— This paper presents an antenna pattern correction technique, which is based on an adaptive array algorithm. In the method, the antenna pattern of the antenna under test (AUT) is measured several times at different positions in the quiet-zone. The corrected antenna pattern is obtained by taking a weighted average of the measured patterns. An array synthesis algorithm is employed for obtaining the averaging weights at each rotation angle of the AUT. The weights are adapted specifically for a given AUT. The adaptive array correction technique is demonstrated in a hologram based compact antenna test range (CATR) at 310 GHz with both a synthetic antenna and a physical test antenna. For verification, the accuracy provided by the adaptive array correction technique is compared to that provided by uniform weighting.**

***Index Terms*—Antenna measurements, compact range, error compensation, submillimeter wave measurements.**

I. Introduction

THE measurement accuracy of a compact antenna test range (CATR) is limited by the level of spurious signals. The spurious signal level should be much lower than the side lobe level of the antenna under test (AUT). However, this requirement can be mitigated by employing antenna pattern correction techniques. One potential correction method is the antenna pattern comparison (APC) [1]. The APC was originally developed for estimating the reflectivity level of an antenna test range, but it can also be used for pattern correction. In the APC method, the antenna pattern is measured several times at different locations in the quiet-zone. The corrected pattern is obtained by combining the measured patterns.

Several methods for obtaining the corrected pattern from the APC data have been developed. In the virtual array method, the antenna pattern of the AUT is measured twice at different positions in the quiet-zone [2]. The antenna is kept in place during the first measurement, whereas it is displaced as a function of the rotation angle during the second measurement. The displacement is adjusted so, that at each rotation angle, the measurement points form a virtual array, whose array factor has a peak in the direction of the desired plane wave and a null in the main beam direction.

Van Norel and Vokurka have introduced a method which they call advanced or novel antenna pattern comparison (NAPC) [3]. The method employs a circle fitting algorithm [4] to the measured data obtained with the conventional APC. In this technique, it is assumed that the received signal at each rotation angle of the AUT is a vector sum of the direct (desired) signal and a spurious signal, which is received through the main beam. The received vectors at each measurement point are normalized so, that the direct signal components are in phase. The normalized vectors span a circle, whose radius equals to the amplitude of the spurious signal and the center equals to the direct signal.

An antenna pattern correction technique, which is based on an adaptive array, is presented in [5]. In this technique, the directions of the spurious signals are estimated with MUSIC algorithm [6] at each rotation angle of the AUT. Then a virtual array, whose array factor is null towards the spurious signals is synthesized.

Far field conditions are assumed in all of these techniques. However, when measuring highly directive antennas, the spurious signals usually originate from the near-field of the AUT because the far-field criterion of an electrically large antenna can not be easily satisfied. When a spurious signal originates from the near-field, it contains several plane wave components instead of one. In the virtual array methods, the array factor should have a broad null towards the scatterer in order to completely filter a spurious signal out. In addition, the MUSIC algorithm does not perform well in the near-field conditions. Other challenges with the MUSIC are that the signals in the test range are strongly correlated and that several snapshots from the quiet-zone field are difficult to obtain. The NAPC suffers from the near-field conditions as well. As the amplitude of the spurious signal is not constant, the received signals do not span a circle when plotted over several positions.

In this paper, we present an antenna pattern correction technique, which is based on an adaptive array algorithm. The

Manuscript received June 14, 2006. This work was supported in part by the Center-of-Excellence program of the Academy of Finland and Tekes, and by the Foundation of the Finnish Society of Electronic Engineers, by the Foundation for Commercial and Technical Sciences, by the Foundation of Technology, by the Jenny and Antti Wihuri Foundation, and by the Graduate School of Electrical and Communications Engineering of TKK.

The authors are with the MilliLab and Radio Laboratory/SMARAD, Helsinki University of Technology, Espoo FI-02015 TKK, Finland.

method employs an array synthesis algorithm for obtaining averaging weights for the measured antenna patterns at each rotation angle of the AUT. The weights are synthesized specifically for a given AUT and therefore high correction accuracy is achieved. The method performs well also if the distortions originate either from broad angular range or from the near-field of the AUT.

The principle of the method is presented in Section II. The test procedure and measurement setup are introduced in Section III. Results are presented in Section IV and conclusions in Section V.

II. Adaptive Array Correction

Let us consider a measurement, in which the antenna pattern of the AUT is measured several times at different spatial locations. The measured results form a linear virtual antenna array at each rotation angle of the AUT as shown in Figure 1. The array pattern (the antenna pattern of the virtual antenna array) at the AUT rotation angle of α can be calculated from

$$P_{ap}(\theta) = P_{af}(\theta) P_{AUT}(\theta - \alpha), \quad (1)$$

where P_{af} is the array factor and P_{AUT} is the antenna pattern of the AUT. The desired plane wave (the measured signal) arrives from the direction of $0°$ whereas the spurious signals arrive from other directions. Therefore, it is desirable to form an array pattern, which receives the desired signal as effectively as possible and attenuates signals arriving from other directions as much as possible. In the proposed adaptive array correction technique, such an array factor P_{af} is designed, that the array pattern P_{ap} has high directivity towards the desired signal and very low directivity to other directions.

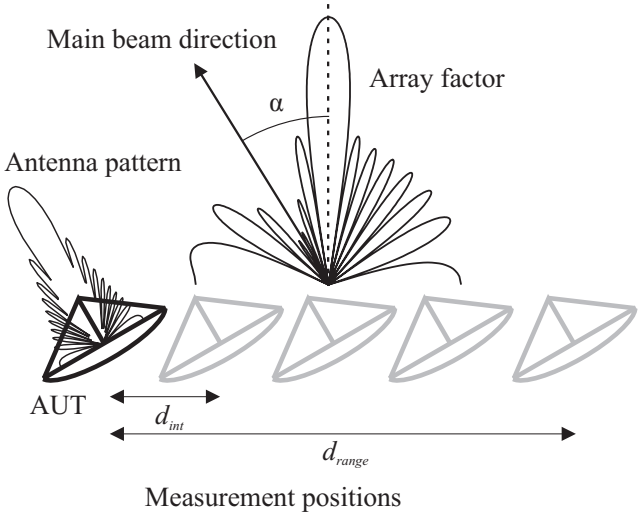

Figure 1. A linear virtual antenna array is formed when the antenna pattern is measured at several locations in the quiet-zone. The figure is not to scale.

A. Measurement Positions

The measurement positions (i.e., the element spacing) define the angular (or wave number range), in which the antenna pattern correction can be accurately performed. In some cases it might be optimal to use arrays with non-uniform element spacing, but in the following we discuss only uniformly spaced arrays. Basically, the displacement interval d_{int} defines the largest angle, in which the correction can be performed, whereas the displacement range d_{range} defines the width of the main beam of the array factor and thus also the smallest angle in which the correction can be performed. If the weighting is uniform, the first null in the array factor occurs at

$$\theta_{min} = \arcsin\frac{\lambda}{d_{range}} \approx \frac{\lambda}{d_{range}}. \quad (2)$$

This is approximately the smallest angle, in which the correction can be fully performed. If the displacement interval does not satisfy the fundamental sampling criterion of $\lambda/2$, the array factor has higher order grating lobes due to aliasing effect. In such case, the main beam of the array factor repeats at the directions of

$$\theta_{max} = \arcsin\frac{n\lambda}{d_{int}}, \quad n = \pm 1,2,3,... \quad (3)$$

as shown in Figure 2. The correction around these directions is not possible.

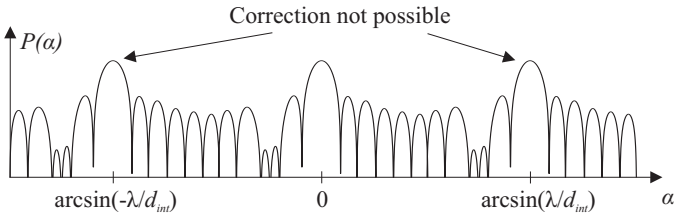

Figure 2. An example of the array factor with higher order grating lobes.

The required positioning accuracy in this method is the same as that required in planar near-field measurements. The probe positioning accuracy requirements in planar near-field measurements are considered in [7].

B. Array Synthesis

The easiest way to control the array factor is to weight antenna elements with known window functions. Different window functions are introduced for example in [8]. Basically, when selecting the window function, one must compromise between the side lobe level and the main beam width of the array factor.

More sophisticated array factors can be synthesized using array synthesis algorithms, such as an algorithm based on alternating projections [9], [10]. Implementation described in [9] is based on Fourier-transform and [10] describes a matrix-inversion based implementation. The matrix-inversion approach may be more convenient as it allows non-uniform element spacing and non-isotropic element patterns.

In the array synthesis, a mask, i.e., lower and upper limits

M_l and M_u for the array pattern (the antenna pattern of the synthesized virtual antenna array) is first defined. Limits can also be defined for the element weights, but this is not needed in this implementation as any element weights are realizable. The iteration begins from the initial guess for the element weights $\mathbf{w}_0$. The corresponding array pattern is calculated with

$$\begin{bmatrix} P_{ap}(\mathbf{u}_{r,1}) \\ P_{ap}(\mathbf{u}_{r,2}) \\ \vdots \end{bmatrix} = \begin{bmatrix} g(\mathbf{u}_{r,1}) e^{jk\mathbf{r}_1\cdot\mathbf{u}_{r,1}} & g(\mathbf{u}_{r,1}) e^{jk\mathbf{r}_2\cdot\mathbf{u}_{r,1}} & \cdots \\ g(\mathbf{u}_{r,2}) e^{jk\mathbf{r}_1\cdot\mathbf{u}_{r,2}} & g(\mathbf{u}_{r,2}) e^{jk\mathbf{r}_2\cdot\mathbf{u}_{r,2}} & \cdots \\ \vdots & \vdots & \ddots \end{bmatrix} \begin{bmatrix} w_1 \\ w_2 \\ \vdots \end{bmatrix}$$

or

$$\mathbf{P}_{ap} = \mathbf{G}\mathbf{w}, \tag{4}$$

where $\mathbf{G}$ is the array response matrix, g is the element pattern, k is the wave number, $\mathbf{u}_r$ is the unit direction vector and $\mathbf{r}$ is the location vector. A projector operator $\mathcal{P}$ is then applied to the array pattern. At points, in which the array pattern is not within the mask, the array pattern is replaced with the limit values as

$$\mathcal{P}P_{ap}(\mathbf{u}_r) = \begin{cases} M_u(\mathbf{u}_r), & |P_{ap}(\mathbf{u}_r)| > M_u(\mathbf{u}_r) \\ P_{ap}(\mathbf{u}_r), & M_l(\mathbf{u}_r) \le |P_{ap}(\mathbf{u}_r)| \le M_u(\mathbf{u}_r) \\ M_l(\mathbf{u}_r), & |P_{ap}(\mathbf{u}_r)| < M_l(\mathbf{u}_r) \end{cases}. \tag{5}$$

The limited array pattern is transformed back to the element weights by using a pseudo-inverse of the array response matrix. The iteration formula for the array weights is

$$\mathbf{w}_{n+1} = \left(\mathbf{G}^*\mathbf{G}\right)^{-1}\mathbf{G}^*\mathcal{P}\mathbf{G}\mathbf{w}_n, \tag{6}$$

where * denotes complex conjugate transpose.

The element pattern, i.e., the antenna pattern of the AUT is used in the array synthesis. The antenna pattern of the AUT is not exactly known, but an estimate of it is obtained by uniformly averaging the measured patterns. This estimated pattern is then used in the array synthesis as an element pattern. As the antenna pattern of the AUT is shifted according to the antenna rotation angle, there is possibly no information about the antenna pattern in the whole angular region in which the array pattern is synthesized. Therefore, the antenna pattern outside the measured region has to be estimated. For example, we estimate the antenna pattern of the AUT to be -50 dB at the angular range that is not measured.

C. Mask for the Synthesized Array Pattern

With the alternating projections method, one must define the mask for the array pattern to be synthesized. The realizable limits depend on the antenna pattern of the AUT, the measurement positions of the AUT, and the number of the measurements. No simple rule for the limits can be defined, but one should obtain a rough knowledge about realizable limits before defining them.

The angular interference spectrum of the test range can be taken into account when defining the limits for the synthesized array pattern. The angular interference spectrum is estimated from the measured antenna patterns using the APC technique [1], which is most suitable with high-gain antennas. The estimated angular interference spectrum depends on the test antenna and the measurement positions, and it is an experienced interference spectrum in the particular measurement. In our implementation, the directions of high interference are attenuated more than directions of a low interference level. The smoothed interference spectrum is used as an upper limit for the synthesized array pattern. However, only interference levels above -40 dB are taken into account. The upper limit for the synthesized array and the reflectivity level in a test case is depicted in Figure 3.

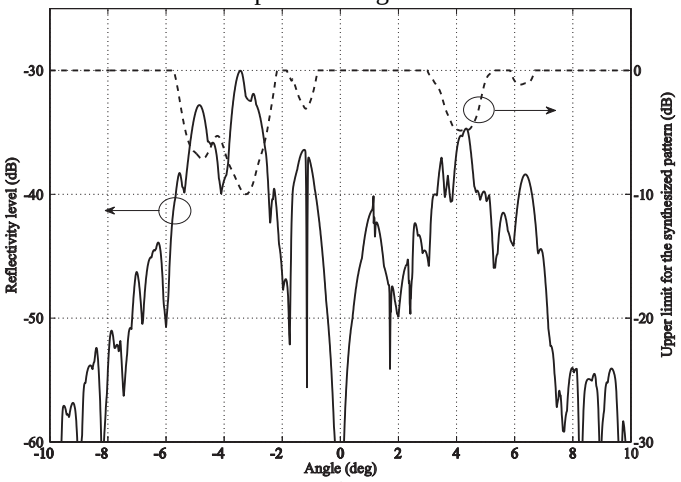

Figure 3. The estimated angular interference spectrum (solid) and the upper limit for the synthesized array pattern (dashed).

The lower limit is defined to be -0.1 dB from $-0.1°$ to $0.1°$ and 0 ($-\infty$ dB) elsewhere. In addition, the array factor is normalized so that the broadside gain is constant at different rotation angles. Figure 4 shows an example of the element pattern, synthesized array factor, and the array pattern at the antenna rotation angle of $-5°$.

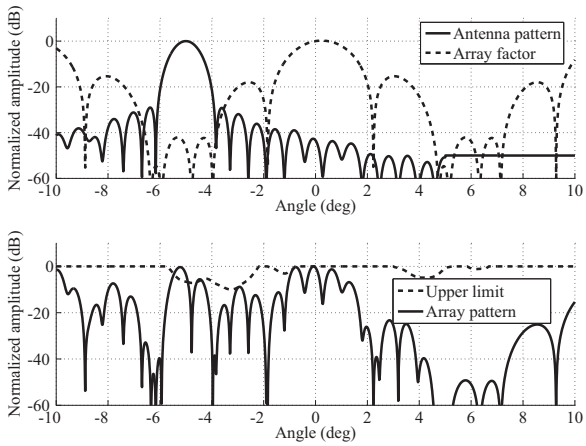

Figure 4. Array factor in the test case with the synthetic antenna at the antenna rotation angle of $-5°$. The upper graph presents the synthesized array factor (dashed) and the element pattern (solid) (i.e., the antenna pattern shifted to $-5°$). The lower graph presents the array pattern (solid) and the upper limit for array pattern (dashed).

D. Applicability of the method

The lower the side lobe level of the AUT, the higher is the required measurement accuracy. Therefore antenna pattern correction techniques are usually needed when measuring low side lobe and high gain antennas. The current implementation of the proposed method is limited to such antennas, because the angular interference spectrum is estimated with the APC technique. However, the adaptive array correction technique itself is very general and it can be used with low gain antennas as well, if the angular interference spectrum is estimated accordingly.

III. Test Procedure and Measurement Setup

The adaptive array correction technique is demonstrated in two ways: by measuring antenna patterns of a synthetic antenna and a physical test antenna. The antenna pattern of the physical test antenna is measured conventionally by rotating the antenna in the quiet-zone, whereas the tests with the synthetic antenna are based partly on measurements (measured quiet-zone field) and partly on simulations.. Tests with the physical antenna are needed to verify the method. The resulting correction accuracy of the method can be defined from the tests with the synthetic antenna, as the true antenna pattern of the synthetic antenna can be analytically calculated. The measurements are performed in both cases in a hologram based compact antenna test range [11]–[13] at 310 GHz. The hologram operation is intentionally distorted by attaching plastic and metal strips on the hologram surface. The distortions are seen approximately at the angles of $5°$ and $-5°$ from the AUT. The physical test antenna is measured conventionally by rotating the AUT in the test zone. The tests with the synthetic antenna are based on the measured quiet-zone field and on the simulated antenna pattern measurements. The two-dimensional quiet-zone field is first probed with a planar scanner. The antenna pattern measurements are then simulated by calculating the measured antenna patterns with the equation

$$P_{\text{meas}}(k_x, k_y) = \iint E_{\text{qz}}(x, y) E_{\text{aper}}(x, y) e^{-j(k_k x + k_y y)} dxdy \,, \quad (7)$$

where E_{qz} is the measured quiet-zone field, E_{aper} is the simulated aperture field of the synthetic antenna, and k_x and k_y are *x*- and *y*-components of the wave vector.

Both the synthetic antenna and the physical antenna have similar geometry. The antennas are based on a single $90°$ offset fed reflector. The reflector diameter is 76.2 mm and its effective focal length is 127 mm. The illumination of the antennas is Gaussian with an edge taper of -12 dB in the plane of symmetry. A commercially available optical mirror is used as a reflector in the physical antenna. The supporting structures are covered with absorbers in order to get good correspondence between the measurements and simulations. The aperture field of the synthetic antenna is simulated with GRASP8W-S program[1].

The antenna patterns of both antennas are measured 7 times. The displacement interval is 5 mm and range 30 mm with the synthetic antenna. The displacement intervals with the physical antenna are accurately known and they are approximately 5 mm (within 0.5 mm). The smallest angle, in which the correction can be performed, is approximately $1.8°$ and the first direction in which the correction can not be performed is $11°$.

For comparison, the accuracy provided by the method is compared to the accuracy provided by the conventional APC. In the APC, the measured patterns are averaged with uniform weighting.

IV. Experimental Results

A. Quiet-Zone Fields

The quiet-zone field is distorted during the antenna measurements for demonstration. Horizontal cuts of the distorted quiet-zone fields, which are used with the synthetic and physical antennas, are depicted in Figures 5 and 6, respectively.

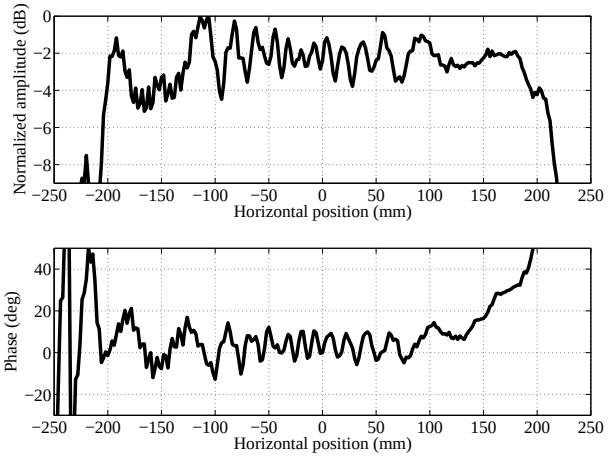

Fig. 5. A horizontal cut of the distorted quiet-zone field used with the synthetic antenna.

[1] http://www.ticra.com

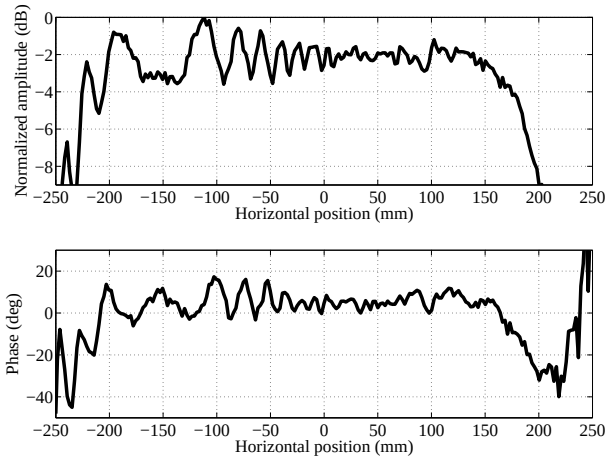

Fig. 6. A horizontal cut of the distorted quiet-zone field used with the test antenna.

Both distorted quiet-zones have approximately a 2-dB ripple in amplitude and a 15º-ripple in phase, peak-to-peak in the aperture of the AUT.

B. Antenna Pattern Correction

The antenna patterns of the virtual antenna are depicted in Figure 7. The measured antenna pattern has spurious side lobes from $-7°$ to $-3°$ and from $4°$ to $7°$. The largest error occurs approximately at $-4°$, where the spurious side lobe level is 18 dB above the true -40 dB level. The averaging with the uniform weighting corrects the antenna pattern approximately with an accuracy of 2.5 dB. The accuracy provided by the adaptive array correction is better than that: the largest error being 0.4 dB. The errors in the corrected patterns are depicted in Figure 8. The corrected pattern with adaptive weighting introduces errors that are in most of the directions from 10 to 20 dB lower than the errors in the corrected pattern obtained with the uniform weighting. An exception occurs at very small angles, where the accuracy provided by the uniform weighting is better. This is natural, as the narrowest main beam of the array factor is obtained with uniform weighting enabling the most accurate correction at small angles. The adaptive array technique may perform worse in these directions if the adaptive array algorithm is converged to a local minimum instead of the global minimum. Another reason may be too small number of the iteration steps in the array synthesis.

The antenna patterns of the physical test antenna are shown in Figure 9. The largest deviation between the non-corrected and the simulated antenna patterns occurs around $-4°$ where the measured pattern is approximately 15 dB above the simulated -40 dB level. Both corrected antenna patterns correspond well with the simulated pattern. The corrected pattern obtained with uniform weighting deviates 3 dB from the simulated pattern at the maximum. The maximum deviations occur at $-4°$ and $8°$. The corrected antenna pattern obtained with adaptive weighting corresponds slightly better to the simulated pattern. It deviates less than 2 dB from the simulated pattern and corresponds well to the simulated pattern also at the angles of $-4°$ and $8°$, where the pattern obtained with uniform weighting has large deviations.

V. Conclusion

A new antenna pattern correction method is presented. The method employs APC data, and it is based on an adaptive array algorithm. The accuracy provided by the method is found to be better than the accuracy provided by simple uniformly weighted averaging. The novel method has been verified at 310 GHz with both a synthetic antenna and a physical test antenna in a hologram based CATR. The method is found to perform well also if the distortions originate from broad angular range or from the near-field of the AUT.

Acknowledgment

The authors gratefully acknowledge Mr. E. Kahra and Mr. H. Rönnberg for help in the manufacturing the test antenna and other fine-mechanical parts, and Dr. J. Häkli, Mr. T. Koskinen and Dr. A. Lönnqvist for their contribution in developing the hologram based compact antenna test range at TKK.

References

[1] J. Appel-Hansen, “Reflectivity level of radio anechoic chambers,” *IEEE Transactions on Antennas and Propagation*, vol. AP-21, no. 4, pp. 490 – 498, July 1973.

[2] W. D Burnside and I. J. Gupta, “A method to reduce signal errors in antenna pattern measurements,” *IEEE Transactions on Antennas and Propagation*, vol. 42, no. 3, pp. 399 – 405, Mar. 1994.

[3] J. van Norel and V. J. Vokurka, “Novel APC-methods for accurate pattern determination,” *Proceedings of the 15th Annual Antenna Measurement Techniques Association (AMTA) Meeting & Symposium, USA*, 1993, pp. 385 – 389.

[4] I. Kåsa, “A circle fitting procedure and its error analysis,” *IEEE Transactions on Instrumentation and Measurement*, vol. 25, pp. 8–14, Mar. 1976.

[5] M. D. Migliore, “Filtering environmental reflections in far-field antenna measurement in semi-anechoic chambers by an adaptive pattern strategy,” *IEEE Transactions on Antennas and Propagation*, vol. 52, no. 4, pp. 1112 – 1115, Apr. 2004.

[6] R. Schmidt, “Multiple emitter location and signal parameter estimation,” *IEEE Transactions on Antennas and Propagation*, vol. 34, no. 3, pp. 276–280, Mar. 1986.

[7] A. C. Newell, “Error analysis techniques for planar near-field measurements,” *IEEE Transactions on Antennas and Propagation*, vol. 36, no. 6, June 1988.

[8] F. J. Harris, “On the use of windows for harmonic analysis with the discrete Fourier transform,” *Proceedings of the IEEE*, vol. 66, no. 1, pp. 51 – 83, Jan. 1978.

[9] O. M. Bucci, G. Franceschetti, G. Mazzarella, and G. Panariello, “Intersection approach to array pattern synthesis,” Proceedings of the IEE, vol. 137, no. 6, pt. H, pp. 349 – 357, Dec. 1990.

[10] E. Botha and D. A. McNamara, “Conformal array synthesis using alternating projections, with maximal likelihood estimation used in one of the projection operators,” *IEE Electronics Letters*, vol. 29, no. 20, pp. 1733 – 1734, Sept. 1993.

[11] T. Hirvonen, J. Ala-Laurinaho, J. Tuovinen, and A.V. Räisänen, “A compact antenna test range based on a hologram,” *IEEE Transactions on Antennas and Propagation*, vol. 45, no. 8, pp. 1270–1276, Aug. 1997.

[12] J. Häkli, T. Koskinen, A. Lönnqvist, J. Säily, J. Mallat, J. Ala-Laurinaho, V. Viikari, A. V. Räisänen, and J. Tuovinen, “Testing of a 1.5 m reflector antenna at 322 GHz in a CATR based on a hologram,”

IEEE Transactions on Antennas and Propagation, vol. 53, no. 10, pp. 3142–3150, Oct. 2005.

[13] A. Lönnqvist, T. Koskinen, J. Häkli, J. Säily, J. Ala-Laurinaho, J. Mallat, V. Viikari, J. Tuovinen, and A. V. Räisänen, "Hologram-based compact range for submillimeter wave antenna testing," *IEEE Transactions on Antennas and Propagation*, vol. 53, no. 10, pp. 3151–3159, Oct. 2005.

Ville Viikari (S'04) was born in Espoo, Finland, in 1979. He received the Master of Science (Tech.) and Licentiate of Science (Tech.) degrees in Electrical Engineering from the Helsinki University of Technology (TKK), Espoo, Finland, in 2004 and 2006, respectively. He is currently working toward the Doctor of Science (Tech.) degree at TKK.

Since 2001, he has been a Trainee, Research Assistant, and Research Engineer with the Radio Laboratory (TKK). His current research interest is the development of the antenna measurement techniques at sub-millimeter wavelengths.

Veli-Matti Kolmonen was born in Rovaniemi, Finland, in 1979. He received the degree of Master of Science in Technology from Helsinki University of Technology (TKK), Espoo, Finland, in 2004. Since 2003 he has been with the Radio Laboratory, TKK, first as a Research Assistant and later as a Researcher. His current research interests include radio channel measurements and modeling.

Jari Salo received the degrees of Master of Science in Technology and Licentiate of Science in Technology from Helsinki University of Technology (TKK) in 2000 and 2003, respectively. From 2001 to 2002 he was with Bitville Oy. Since November 2002, he has been with the Radio Laboratory of TKK where he is currently working toward the doctoral degree.

Antti V. Räisänen (S'76-M'81-SM'85-F'94) received the Doctor of Science (Tech.) degree in Electrical Engineering from the Helsinki University of Technology (TKK), Finland, in 1981. Dr. Räisänen was appointed to the Professor Chair of Radio Engineering at TKK in 1989, after holding the same position as an acting professor in 1985 and 1987–1989. He has held visiting scientist and professor positions at the Five College Radio Astronomy Observatory (FCRAO) and University of Massachusetts, Amherst (1978–79, 80, 81), at Chalmers University of Technology, Göteborg, Sweden (1983), at the Department of Physics, University of California, Berkeley (1984–85), at Jet Propulsion Laboratory and California Institute of Technology, Pasadena (1992–93), and at Paris Observatory and University of Paris 6 (2001–02).

Currently, Dr. Räisänen is supervising research in millimeter-wave components, antennas, receivers, microwave measurements, etc. at TKK Radio Laboratory and MilliLab (Millimetre Wave Laboratory of Finland – ESA External Laboratory). The Smart and Novel Radios Research Unit (SMARAD) led by Dr. Räisänen at TKK, obtained in 2001 the national status of Center of Excellence in Research from the Academy of Finland after competition and international review. He has authored and co-authored some 400 scientific or technical papers and six books, e.g. *Radio Engineering for Wireless Communication and Sensor Applications* (Massachusetts: Artech House, 2003, with A. Lehto). He also co-authored chapter *Radio-Telescope Receivers* with M.E. Tiuri in J.D. Kraus: *Radio Astronomy* (Powell, OH: Cygnus-Quasar Books, 2nd edition, 1986).

Dr. Räisänen was Secretary General of the 12th European Microwave Conference in 1982. He was Chairman of the IEEE MTT/AP Chapter in Finland from 1987 to 1992. He was Conference Chairman for the 22nd European Microwave Conference in 1992 and for the 2nd ESA Workshop on Millimetre Wave Technology and Applications: antennas, circuits and systems in 1998, and Co-Chair for the 3rd ESA Workshop on Millimetre Wave Technology and Applications: circuits, systems, and measurement techniques in 2003. In 2006, he is Conference Chairman of the International Joint Conference of the 4th ESA Workshop on Millimetre-Wave Technology and Applications, the 8th Topical Symposium on Millimeter Waves TSMMW2006, and the 7th MINT Millimeter-Wave International Symposium MINT-MIS2006. During 1995–97 he served in the Research Council for Natural Sciences and Engineering, the Academy of Finland. From 1997 to 2000 he was Vice-Rector for Research and International Relations of TKK. He served as an Associate Editor of the *IEEE Transactions on Microwave Theory and Techniques* from 2002 to 2005.

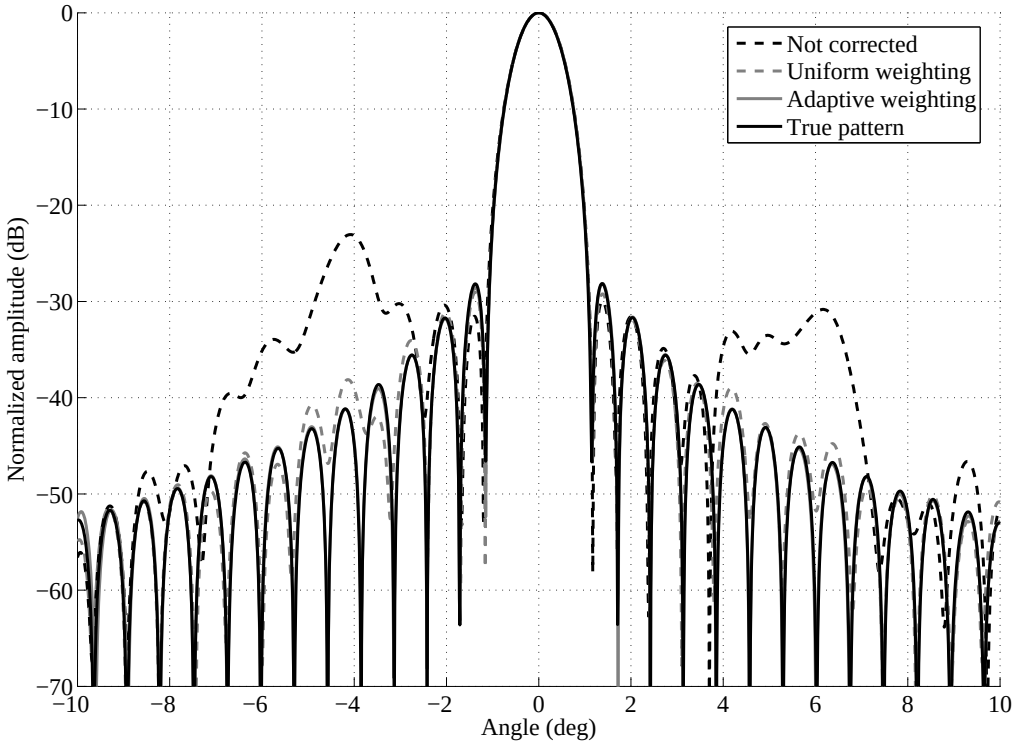

Figure 7. Antenna patterns with the synthetic antenna. The solid black line is the true pattern, the dashed black line is the non-corrected pattern, the dashed gray line is the corrected pattern obtained with uniform weighting, and the solid gray line is the corrected pattern obtained with adaptive weighting.

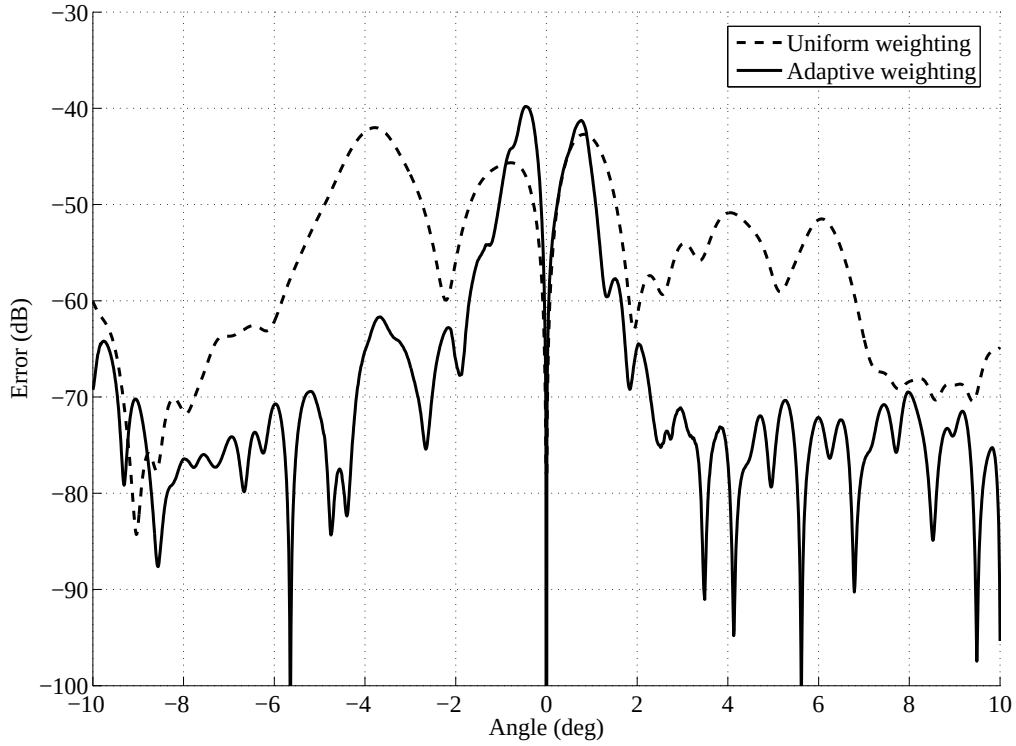

Figure 8. Error in the corrected antenna patterns. The dashed black line is the error in the corrected antenna pattern obtained with uniform weighting and the solid black line is the error in the corrected antenna pattern obtained with adaptive weighting.

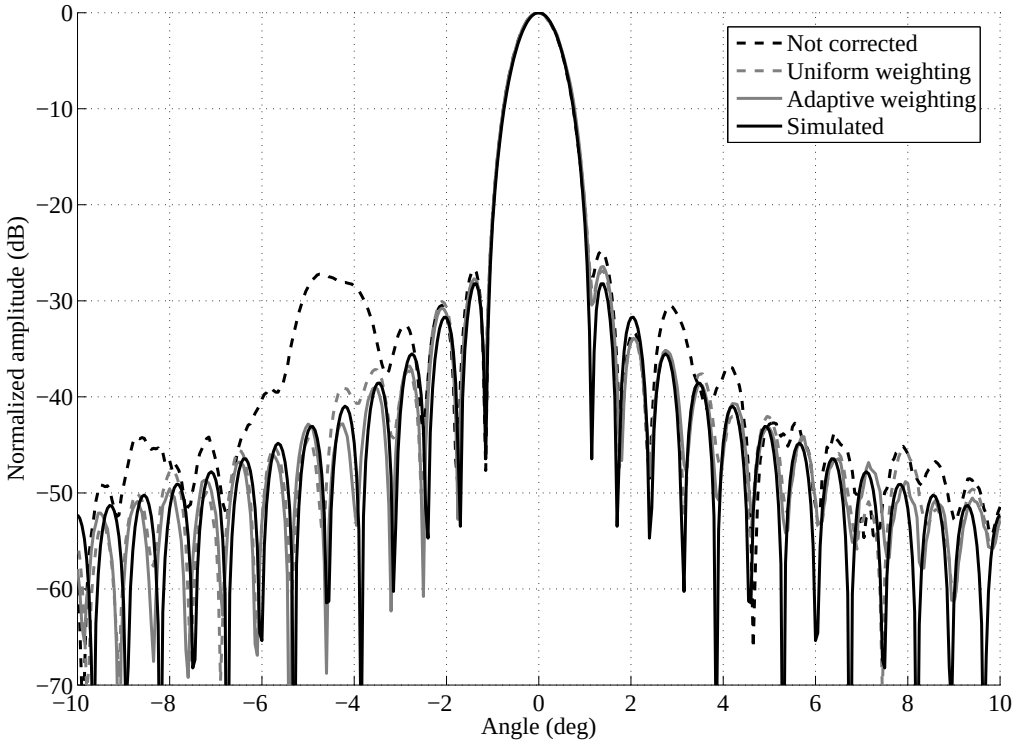

Figure 9. Antenna patterns with the test antenna. The solid black line is the simulated pattern, the dashed black line is the non-corrected pattern, the dashed gray line is the corrected pattern obtained with uniform weighting, and the solid gray line is the corrected pattern obtained with adaptive weighting.